Turkish Journal of Earth Sciences

Manuscript 1916

Mapping of lithological units in the western part of the Eastern Taurides (Türkiye) using ASTER images

DENİZ HOZATLIOĞLU

ÖMER BOZKAYA

SEDAT İNAL

KAAN ŞEVKİ KAVAK

TÜBİTAK

Turkish Journal of Earth Sciences

http://journals.tubitak.gov.tr/earth/

Research Article

Turkish J Earth Sci
(2024) 33: 362-383

doi:10.55730/1300-0985.1916

Mapping of lithological units in the western part of the Eastern Taurides (Türkiye) using ASTER images

Deniz HOZATLIOĞLU[1,*], Ömer BOZKAYA[2], Sedat İNAL[3], Kaan Şevki KAVAK[1]

[1]Department of Geological Engineering, Sivas Cumhuriyet University, Sivas, Turkiye
[2]Department of Geological Engineering, Pamukkale University, Denizli, Turkiye
[3]MTA Central Anatolia Regional Directorate, Sivas, Turkiye

Received: 25.07.2023 • **Accepted/Published Online:** 10.01.2024 • **Final Version:** 19.03.2024

Abstract: The Eastern Taurides, which form the imbrication and nappe zone in the northernmost part of the Arabian platform, are located within the Southeastern Anatolian Orogenic Belt. In the present study, spectral enhancement methods such as band ratioing, minimum noise fraction (MNF), relative band depth (RBD), and supervised classification were applied to ASTER (Advanced Spaceborne Thermal Emission and Reflection Radiometer) images of metamorphic massifs, ophiolites, and sedimentary rocks outcropping in the western part of the Eastern Taurides (Göksun, Afşin, and Ekinözü regions). With these methods, the aim was to distinguish geological units from each other accurately. In the study area, arid climatic conditions with relatively poor vegetation, allowing for precise visual interpretations, play a significant role. Vegetation and water bodies were also masked before these procedures. In the Göksun, Afşin, and Ekinözü regions, metamorphic rocks of phyllite, schist, and gneiss types, which underwent metamorphism during the Upper Cretaceous and Eocene periods, are observed. The geologically dominant minerals in these rocks include silica, mica (muscovite, phengite, biotite), chlorite (clinochlore, chamosite), kaolinite, and carbonates (calcite, dolomite). These rocks are accompanied by ophiolitic, volcanic/volcano-sedimentary, and plutonic igneous rocks. Due to geological events during the closure of the Neotethys Ocean and continental collision in the area, it became evident that the lithological diversity from various rock groups was reflected in the ASTER images, in addition to field observations. Image processing analyses applied to the ASTER sensor images, rich in short-wave infrared (SWIR) and thermal infrared (TIR) bands on the Terra platform, revealed distributions of clay, sulfate, carbonate, iron oxide, and silica minerals. The highest geological differentiation potential was observed through ASTER 643 (RGB) and ASTER 13,12,10 (RGB) false-color composites, as well as ASTER 456 (RGB) minimum noise fraction (MNF) analyses and, especially, relative band depth processes.
Relative band depth processes were employed to identify epidote-chlorite-amphibole, calcite-chlorite-amphibole, alunite-kaolinite-pyrophyllite, muscovite, and silica minerals. The application of these processes revealed lithologies that strongly feature these minerals. Specifically, the goal was to differentiate rock units containing kaolinite, muscovite, phengite, chlorite, and epidote minerals belonging to AlOH and FeOH groups and elucidate their compositions. Moreover, rocks containing primarily quartz and feldspar were distinguished using ASTER TIR bands. The obtained data revealed that mineralogical and corresponding lithological spatial distributions, as depicted by ASTER images, could play a crucial role in geological mapping, particularly in regions where mapping is challenging due to geographical conditions.

Key words: The Eastern Taurides, spectral enhancement, metamorphism, ASTER, relative band depth, band ratioing

1. Introduction

The Anatolian Plate constitutes a tectonic mosaic with continental slices that rifted and separated from the African/Arabian Plate during continental collision, eventually adding to the Eurasian Plate (Yılmaz et al., 2023). In the course of this collision, the Paleotethys Ocean closed during the Late Paleozoic-Early Mesozoic period, followed by the closure of the Neotethys Ocean during the Mesozoic-Cenozoic period (Şengör and Yılmaz, 1981; Yılmaz, 2019). The Southeast Anatolian Orogenic Belt constitutes the southernmost component of the Anatolian Orogen and extends eastward to the Zagros Mountains and the Oman-Makran subduction system (Figure 1).

In the Southeast Anatolian Orogenic Belt, where metamorphic massifs are cropped out, three tectonic belts were differentiated by Yılmaz and Yiğitbaş (1990) and Yılmaz (1993) from south to north as the Arabian Platform, Imbrication Zone, and Nappe Zone (Yılmaz and Yiğitbaş, 1990). Among these, the Arabian Platform is characterized by Cambrian-Paleogene-aged autochthonous sedimentary rocks (Southeast Anatolian Autochthonous Unit), while the Nappe Zone, where the study area is located, is

* Correspondence: dhozatlioglu@cumhuriyet.edu.tr

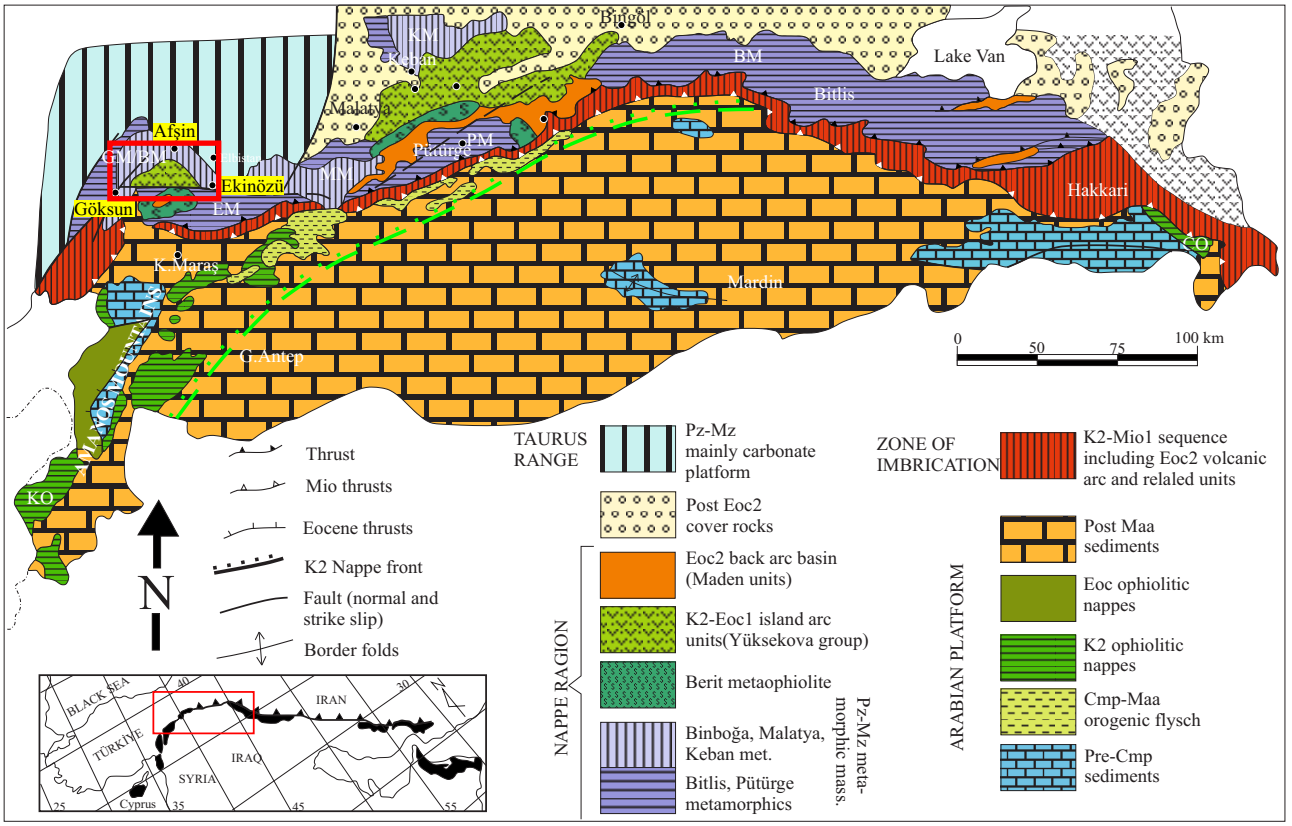

Figure 1. Geological map of the Southeast Anatolian Region (Modified from Yılmaz et al., 2023). (Pz: Paleozoic, Mz: Mesozoic, Maa: Late Campanian-Early Maastrichtian, Cmp: Upper Campanian-Lower Maastrichtian, K2: Upper Cretaceous, Eoc: late Middle Eocene, Eoc1: late Early Eocene, Eoc2: late Early Eocene–Middle Eocene, Mio1: Early Miocene). The black strip in the inset map shows the suture mountains (Yılmaz, 1993) of the Bitlis-Zagros Orogenic Belt.

characterized by ophiolitic, metamorphic, and volcanic-volcano clastic sedimentary rocks. The Imbrication Zone consists of reverse fault and thrust slices delimiting the northern extension of the Arabian Platform. The Cambrian-Paleogene-aged sedimentary units, which belong to the Eastern Taurus Autochthon (Geyikdağı Unit) outcrop in the northwest of the Nappe Zone (Özgül, 1976). In this region, these units are unconformably overlain by Neogene-Quaternary-aged sedimentary and volcanic rocks. The metamorphic units outcropping in the Göksun, Afşin, and Ekinözü regions in the study area were classified by Özgül (1976) as part of the allochthonous Alanya Units, one of the Taurus Belt tectonic units.

Remote sensing is the study of collecting and interpreting data from a distance without physical contact with the matter. ASTER, a crucial tool for geological remote sensing studies, is a high-performance ground observation sensor operated by Japan (METI) and is positioned on the Terra satellite (Abrams and Hook, 1995; Yamaguchi et al., 1998; Abrams, 2000). ASTER finds applications in various scientific disciplines, including land use/land cover, urban monitoring, urban heat map studies, wetland studies, agricultural monitoring, and forestry, in addition to geosciences. The significance of ASTER images in geosciences is particularly high, being used extensively for geological purposes such as determining rock types, detailed volcanic activity mapping, identifying linear and circular structures, generating hydrothermal alteration areas and mineralogical zone maps, identifying geothermal areas, and obtaining stereoscopic three-dimensional images. Spectral enhancement methods can also be applied to ASTER images (Vincent, 1997; Bierwirth, 2002; Crosta et al., 2003; Rowan and Mars, 2003; Volesky et al., 2003; Gomez et al., 2005; Ninomiya et al., 2005; Gad and Kusky, 2007; Van der Meer et al., 2012; Hewson et al., 2018; Pour et al., 2019; Sekandari et al., 2022; Esmaeilzadeh et al., 2023). This approach allows for the determination of rock and mineral types through the utilization of appropriate band combinations (Bierwirth, 2002; Rowan and Mars, 2003; Volesky et al., 2003; Hewson et al., 2005; Massironi et al., 2008). The Nappe Zone, located in the study area and represented by rock associations with diverse

lithologies, such as ophiolitic, metamorphic, volcanic, and volcanoclastic types, was mapped using satellite images and remote sensing techniques. The obtained data were then compared with field data and geological maps.

The objective of the current study was to unveil the mineralogical-petrographic features of a region that had previously undergone detailed examination, focusing on mineralogical aspects using ASTER images. Accordingly, mineral mapping of the geological units in the region was conducted, utilizing the spectral resolution of the ASTER sensor. The approach involved distinguishing the minerals constituting the metamorphic units through image processing methods.

This study aimed to explore the distribution of mineral zones obtained from ASTER images in a region whose lithological features were previously investigated by Hozatlıoğlu et al. (2020, 2021). Within this context, mineral mapping of the geological units in the region was conducted, utilizing the spectral resolution of the ASTER sensor. The approach involved differentiating the minerals constituting the metamorphic units through image processing methods.

2. Geology of the study area

The mineralogical-petrographic and geochemical features of the Upper Paleozoic-Lower Mesozoic-aged metamorphic rocks in the Göksun, Afşin, and Ekinözü regions located in the western part of the Eastern Taurus belt known as the pre-Alpine tectonic units, were extensively detailed by Hozatlıoğlu et al. (2020, 2021). This study, however, focuses solely on the definition of lithostratigraphic units.

The metamorphic units in the study area are located within the Alanya Unit, encompassing clastic and carbonate rocks formed during the Upper Devonian-Upper Cretaceous age interval. The oldest rock units outcropping in the study area are the Upper Paleozoic (Yoncayolu and Çayderesi formations) and Triassic (Alçılı Formation) aged metamorphites, along with granitoid intrusions cutting through them (Figure 2). This rock assemblage is tectonically overlain by allochthonous and cover units that have not undergone metamorphism above (Yılmaz et al., 1993, 1997). The Upper Paleozoic-Triassic-aged metamorphic rocks and Jurassic-Cretaceous-aged ophiolitic units outcrop extensively in the study area. The units in the study area, with their stratigraphic column section presented in Figure 3, represent the tectono-stratigraphic units of the southern part of the Eastern Taurides (Yılmaz et al., 1993).

The oldest rock units outcropping in the study area are Upper Paleozoic-Triassic-aged metaclastic and metacarbonate rocks metamorphosed under greenschist facies conditions, intersected by Upper Cretaceous-Eocene-aged granitic intrusions (Yılmaz et al., 1993). These metamorphic rock assemblages tectonically pass into the Jurassic-Lower Cretaceous-aged carbonate rocks unaffected by metamorphism above. The Upper Cretaceous-aged Binboğa Formation, containing reefal limestones (Perinçek and Kozlu, 1984), is one of the allochthonous units whose positions in the study area are controversial and is overlain by the Upper Cretaceous-aged olistostromal Kemaliye Formation (Özgül, 1976) with local unconformity. The Upper Cretaceous-aged Dağlıca Complex (Perinçek and Kozlu, 1984), comprising blocks of ophiolite and sedimentary origin, tectonically overlies the Kemaliye Formation. The Jurassic-Cretaceous-aged Göksun ophiolite (Yılmaz et al., 1993), housing intrusions of the Mesozoic-aged Esence granitoid (Yılmaz et al., 1993), is tectonically positioned above these units. The Maden Group (Yılmaz et al., 1993), consisting of Middle Eocene-aged volcano-sedimentary rocks, Neogene-aged sedimentary volcanics, and Quaternary deposits, unconformably covers them.

3. Materials and methods

Optical microscopy (OM) studies were conducted to identify the mineral compositions and textural properties of the rock samples collected from the field. The petrographic features resulting from the relationships within the minerals and matrix texture in the rocks were interpreted. Alongside rock nomenclature, investigations were undertaken into alterations and related occurrences (Hozatlıoğlu et al., 2020).

X-ray diffraction analyses (XRD) were carried out using a Rigaku DMAX IIIC model X-ray diffractometer to determine the bulk and clay size components (< 2 μm) of the samples. Semiquantitative percentages were calculated based on the external standard method of Brindley (1980) using mineral intensity factors proposed by Yalçın and Bozkaya (2002). The polytype of pure or nearly pure illite/K-mica and chlorite minerals was determined using representative peaks suggested by Bailey (1980, 1988).

Geological remote sensing data is a crucial technology employed in regional mapping, structural interpretation, and mineral deposit/oil exploration (Van der Meer et al., 2012). In remote sensing, the interaction of matter with electromagnetic energy occurs at the atomic level, and the behavior of light is represented on the molecular scale through processes like absorption, reflection, and emissivity (Gupta, 2018). Rocks can be correlated with photo interpretation using geological maps in images, while minerals and their components can be recognized based on their absorption values in images. Each mineral can have one or more absorption values unique to itself (Clark et al., 1990; Yamaguchi et al., 1998; Van der Meer et al., 2012). Spectral curves, also known as wavelength-

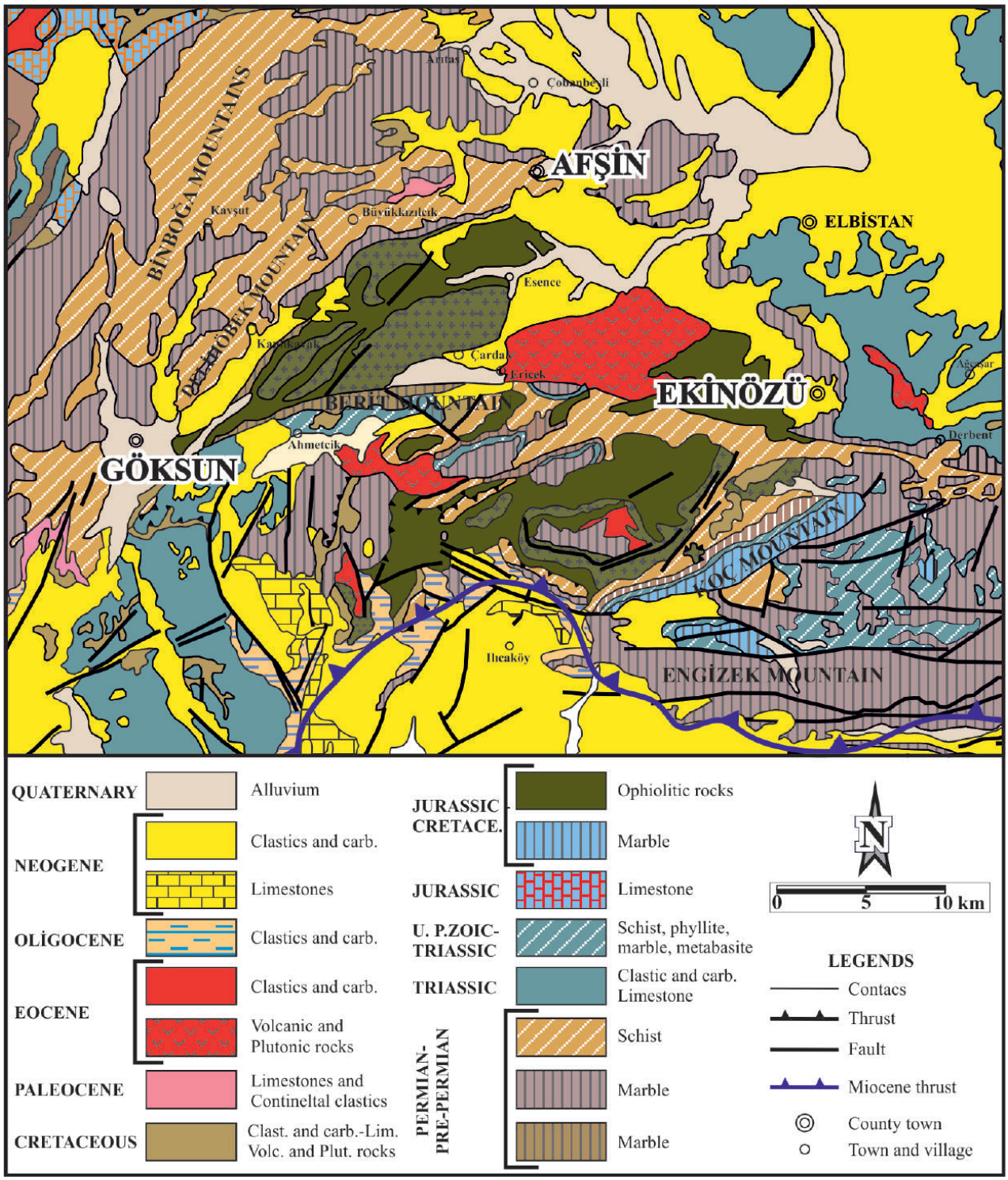

Figure 2. Geological map of the region within the study area (prepared from Bilgiç, 2002 and Ulu, 2002).

reflection curves, are obtained in spectroscopy laboratories, and the associated spectral curves of most minerals were identified in laboratory studies conducted in the early 1970s (Hunt, 1977).

In this study, detailed mineralogical-petrographical and geochemical analyses were supported by visual interpretation and image processing methods. During the execution of these ground truthing efforts, it is noteworthy

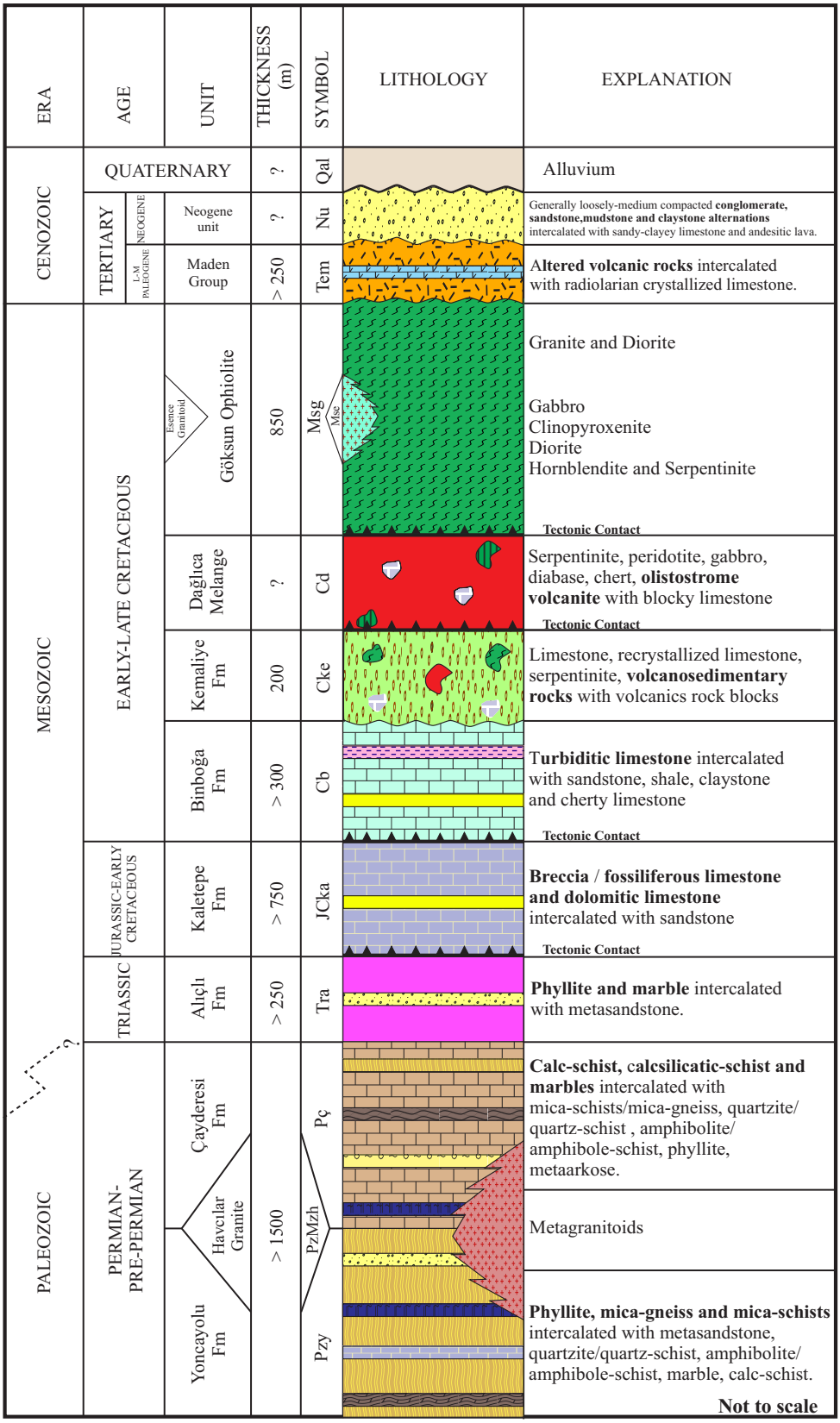

Figure 3. Generalized tectono-stratigraphic columnar section of the southern part of the Eastern Taurus (modified from Yılmaz et al., 1993).

that the boundaries between various rock units and some structural data, such as geological lineaments and faults, in previously created geological maps were consistent with the results obtained from image processing studies. In summary, it can be stated that the spatial and spectral enhancement methods applied after field studies are largely in agreement with the geological map of the region. ASTER relies on properties in the visible-infrared (VNIR) spectral region, where electronic processes in transition metals and various anion groups, such as silicates, oxides, hydroxides, carbonates, and phosphates, exhibit poor absorption for recognizability. Iron is the most recognizable mineral in this region, with Fe^{3+} and Fe^{2+} bearing minerals presenting recognizable absorption at values of 1.3 and 1.6 μm (Clark and Roush, 1984). The short-wave infrared region (SWIR) of the ASTER sensor is crucial for emphasizing the spectral properties of hydroxyls and carbonates, which are abundant in the Earth's crust. Hydroxyl ions are common components found in rock-forming minerals such as clay, mica, and chlorite. They have a fundamental vibrational absorption band around 2.74–2.77 μm and 1.44 μm. On the other hand, carbonates exhibit significant absorption at 1.9, 2.35, and 2.55 μm (Van der Meer et al., 2012). In the thermal infrared region (TIR), minerals stand out with their emissivity values, apart from absorption. Carbonates, nitrites, nitrates, phosphates, sulfates, oxides, and silicates have recognizable emissivity values in this region (Rowan and Mars, 2003; Mars and Rowan, 2010, 2011; Gupta, 2018).

When performing a regional mineralogy mapping with ASTER, it is important to note that it may not offer information as reliably as hyperspectral sensors, and attention should be paid to the following three points. First, water (1) and vegetation (2) were masked in this study due to their ability to mask and alter the surface signals of vegetation and water, respectively.

$$NDWI = \frac{\text{Green}-\text{NIR}}{Green+NIR} \quad NDWI = \frac{\text{B1}-\text{B3}}{B1+B3}$$
$$NDVI = \frac{\text{NIR}-\text{Red}}{NIR+Red} \quad NDVI = \frac{\text{B3}-\text{B2}}{B3+B2} \qquad (1)$$

Secondly, the bands and band ratios of the sensor provide precise amounts and quantitation of minerals. Therefore, ground truthing is also necessary, and this study was conducted based on a database of samples taken from the field, where the stratigraphy and tectonics were already known.

ASTER (Advanced Spaceborne Thermal Emission and Reflection Radiometer) is the fifth sensor on the Terra Platform, offering wide multispectral coverage and high spatial resolution. The spatial resolutions of ASTER images, with 14 bands including visible and near-infrared (VNIR), short-wave infrared (SWIR), and thermal infrared (TIR), are 15 m, 30 m, and 90 m, respectively (Table 1). ASTER is a radiometer with three spectral bands in the VNIR region, from visible to near-infrared. The sensor comprises six bands in the SWIR region, making it particularly valuable for geological applications. TIR is a part of the radiometer that measures the thermal infrared radiation emitted from the Earth with high accuracy and records the surface temperature and surface emissivity. The radiometric resolution of the sensor is 8 bits in VNIR and SWIR bands and 12 bits in TIR bands, with each image covering a width of 60 km. ASTER images are L2 level, with a stereo feature that can produce an elevation model, oriented to the north, and plant and water masks are applied. As the study area spanned four neighboring images, they were mosaicked and made ready for processing with the linear contrast stretching method. Crosstalk correction (Iwasaki et al., 2001; Hewson et al., 2005) was applied to the ASTER image used in the study, and ASTER DEMs were used as a base for image displays. Crosstalk is an unwanted signal and can also be described as an optical or electrical signal that affects the bands of an image. This situation caused quite a problem in ASTER images for a while.

In the study, 1/500,000 scaled geological maps from the General Directorate of Mineral Research and Exploration provided the basis for lithological evaluations performed with the images.

Human eye retina receptors and cones contain three different kinds of pigments sensitive to red, green, and blue light. These lights are combined in the human brain and color vision is achieved (Drury, 2001). Similar to seeing human vision concept, geologists use band combinations with the aid of image processing software. Different wavelengths of the electromagnetic spectrum are assigned to mainly red, green, and blue colors in computers using image processing software. This RGB notation in image processing follows a scientific logic where three different colorless wavelengths merge to appear as a single color representation of the field of view derived from imaging sensors.

Remotely sensed images can be represented as grey-tone images of single bands or as three-band color images, along with various arithmetic combinations of bands. These combinations are achieved by dividing the digital number (DN) of each pixel in one band by that for the corresponding pixel in another band(Drury, 2001). While individual bands of remotely sensed images show the effect of varying illumination due to topography, the effect of this illumination is eliminated by ratioing bands. This ratioing helps reveal an interpretable, well-lit image independent of illumination. Ratioed images also provide a powerful tool for lithological mapping efforts in the field. Spectral curves represented for each lithology in the field, also known as

Table 1. General characteristics of the ASTER detector.

Subsystem		Band no.	Spectral range (μm)	Areal resolution (m)	Primary application areas
VNIR	Visible and near infrared	1	0.52–0.60	15	Geology, iron oxide minerals, mapping coral reefs, digital elevation model, glacier monitoring, classification of land areas and change detection, cloud classification, soil moisture, surface energy balance, residential development, vegetation cover, monitoring volcanoes, mapping of wetlands.
		2	0.63–0.69	15	
		3 N 3 B	0.78–0.86	15	
SWIR	Short-wave infrared	4	1.600–1.700	30	Geology, hydrothermal alteration areas, soil classification, classification of terrestrial areas, change detection, surface energy balance, monitoring volcanoes.
		5	2.145–2.185	30	
		6	2.185–2.225	30	
		7	2.235–2.285	30	
		8	2.295–2.365	30	
		9	2.360–2.430	30	
TIR	Thermal Infrared	10	8.125–8.475	90	Geology, fire monitoring, classification of land areas, change detection, cloud classification, soil moisture, surface energy balance, surface kinematic heat, city development, vegetation, volcano monitoring, mapping of wetlands.
		11	8.475–8.825	90	
		12	8.925–9.275	90	
		13	10.25–10.95	90	
		14	10.95–11.65	90	

reflection-wavelength curve, are obtained by ratioing different wavelengths based on rock compositions.

The Minimum noise fraction (MNF) method used in this study resembles principal component analysis and is employed to reduce noise without degrading data quality (Green et al., 1988; Luo et al., 2016). Excessively correlated bands in multi- or hyperspectral imaging systems lead to data redundancy. MNF helps mitigate this issue.

The relative band depth (RBD) method is designed to identify diagnostic mineral absorption features while minimizing reflectance variations related to topographic slope and albedo differences. RBD images are produced by summing several data channels near an absorption band shoulder and dividing by the sum of several channels located near the band minimum (Brickey et al., 1987; Crowley et. al., 1989; Rowan et al., 2005). They are highly specific and sensitive to the presence of particular mineral absorption features. This technique does not distort or subdue spectral features, as can happen with other data normalization methods.

Another method used in this study is supervised classification, where the user provides a set of labeled training samples for each class of interest. Classifier algorithms use these training samples to learn the characteristics of each class and then apply this knowledge to classify the entire image into specified categories (Richards, 1986).

4. Mineralogy-petrography

The mineralogical-petrographic features of metamorphic rocks in Göksun, Afşin, and Ekinözü regions were extensively discussed by Hozatlıoğlu et al. (2020). Here, a concise description of the relevant metamorphic rocks is provided.

The crenulation folded/sliced phyllite, calcphyllite, and marble lithologies that constitute the metamorphic rocks around Göksun mainly contain calcite, dolomite, quartz, feldspar, and phyllosilicate ($2M_1$ illite/K-mica, II*b* chlorite, paragonite, kaolinite, chlorite-vermiculite/C-V, illite-chlorite/I-C). According to KI and *b*-cell distance data, the metamorphites indicate conditions characteristic of high anchizone-epizone and medium-pressure facies (subgreenschist facies).

The metamorphic rocks around Afşin include phyllite, calc-phyllite, calc-schist, garnet and epidote-mica-schist, chlorite-epidote-amphibole-schist, and tremolite and micaceous marble lithologies, and phyllosilicate minerals consist of illite/K-mica (1*M* biotite, $2M_1$ muscovite, paragonite), II*b* chlorite, C-V, I-C, illite-smectite/I-S and smectite. In addition to mineral associations and textural data, illite/K-mica KI (epizone) and *b*-cell dimension (medium-high pressure facies series) data correspond to subgreenschist-greenschist facies conditions.

The metamorphic rocks around Ekinözü consist of mica-schist and mica-gneiss lithologies containing chlorite-schist, amphibole-schist, garnet, sillimanite, staurolite, and kyanite at lower levels and calcitic and dolomitic marbles containing tremolite, actinolite, biotite, muscovite, and chlorite at upper levels. Micas have trioctahedral composition ranges between muscovite ($2M_1$) and biotite (1*M*) (biotite-celadonite, muscovite-phlogopite, muscovite-ferri-phengite, muscovite-ferrobiotite, Al-phlogopite-Al-annite), whereas chlorites (II*b*) have a trioctahedral composition between chamosite and clinochlore (brunsvigite and diabantite). According to their mineral associations, the metamorphic rocks in the Ekinözü region show metamorphic grades reflecting amphibolite facies conditions at the lower levels rich in metabasic and metapelitic rocks and greenschist facies conditions at the upper levels rich in metacarbonates. Coarse-sized biotite, muscovite, and chlorites are accompanied by C-V, C-S, I-C, and illite-vermiculite/I-V, which indicate very-low-grade metamorphism.

The statistical evaluation results for the rock-forming minerals (XRD-bulk composition) identified in the metamorphic rock groups around Göksun, Afşin, and Ekinözü are presented in Table 2, progressing from west to east in the regions of Göksun, Afşin, and Ekinözü. General average values indicate a decrease in calcite minerals from west to east, while feldspar minerals show an increase. Quartz maintains approximately the same average in each region. Mica and chlorite minerals are most prevalent in the Göksun region and least prevalent in the Afşin region. The statistical assessment of minerals constituting phyllosilicates reveals that smectite, mixed-layer C-V, and C-S minerals were predominantly observed in the Afşin region, whereas illite and mixed-layer I-C minerals were more common in the Göksun region. The analysis also shows an increase in chlorite content from west to east and a decrease in the amount of mixed-layer I-C.

Regarding the mineral zones identified through remote sensing methods in the study area, kaolinite/pyrophyllite (argillic alteration for remote sensing) corresponds to very low-grade metamorphic (subgreenschist facies) pelitic rocks (e.g., metasiltstone, metashale, slate). Sericite/muscovite/illite (phyllic alteration for remote sensing) corresponds to low-grade metamorphic (greenschist facies) rocks like phyllite and schist. Similarly, calcite/chlorite/epidote and epidote/chlorite/amphibole mineral zones correspond to greenschist to low-amphibolite facies metamorphic rocks such as calc-phyllite, calc-schist, schist, and gneiss.

5. Results

5.1. Band combinations

ASTER data can be used to discriminate between rocks belonging to silicate, carbonate, and sulfate mineral groups in the thermal region, with mainly ferric (Fe^{2+}) and ferrous (Fe^{3+}) iron, rare earth elements, Al-OH, Fe, Mg-OH, and HOH mineral groups (Pour et. al., 2019; Rowan and Mars, 2003).

In geological remote sensing, the selection of band combinations is generally aimed at enhancing the display of information content, especially when dissimilar regions of the electromagnetic spectrum are combined. Additionally, by assigning the colors red, green, and blue to the three selected bands, this discrimination power is significantly increased from a spectral perspective. ASTER proves to be a very suitable sensor for this process. By assigning and combining a single band selected from each of the visible, infrared, and thermal infrared components to one of the RGB components, detailed displays with high geological information content are achieved, facilitating meticulous geological mapping in the field.

The ASTER 643 (RGB) image reveals distinct geological features across the study area. In this false color composite,

Table 2. Statistical evaluation results of rock-forming minerals and phyllosilicates in Göksun (G), Afşin (A), and Ekinözü (E) regions (%).

XRD-WR / XRD-CF	Presence frequency			Minimum			Maximum			Arithmetic average			General average *		
	G	A	E	G	A	E	G	A	E	G	A	E	G	A	E
Calcite	78	74	18	3	2	2	100	100	100	53	50	68	41	37	12
Dolomite	15	13	8	2	2	1	24	97	5	8	35	3	1	4	< 1
Quartz	89	83	71	1	1	1	88	42	100	14	14	18	13	12	13
Feldspar	74	68	76	2	5	2	21	61	66	8	25	27	6	17	20
Mica	83	34	35	4	3	5	70	48	72	25	14	36	21	5	12
Chloride	65	55	78	5	3	3	62	36	91	29	14	21	19	8	16
Amphibole	0	32	44	0	5	5	0	75	90	0	43	55	0	14	24
Pyroxene	0	4	6	0	17	3	0	43	22	0	30	10	0	1	1
Epidote	0	6	1	0	12	15	0	14	59	0	13	15	0	1	< 1
Scapolite	0	2	0	0	22	0	0	22	0	0	22	0	0	< 1	0
Tremolite	0	0	1	0	0	59	0	0	59	0	0	59	0	0	1
Hematite	2	13	23	1	1	1	1	9	8	1	4	2	< 1	< 1	1
Smectite	8	40	9	10	15	8	14	70	15	12	45	12	1	18	1
Illite	100	40	68	30	15	5	100	85	100	73	50	63	73	20	42
Chloride	75	50	74	2	10	1	65	65	100	18	30	56	13	15	41
C-V	17	80	44	10	5	6	19	73	44	13	35	19	2	28	8
C-S	4	10	6	33	85	24	33	85	73	33	85	49	1	9	3
I-C	38	20	15	5	20	8	50	20	25	26	20	18	10	4	3
Pg	4	0	0	7	0	0	7	0	0	7	0	0	< 1	0	0
I-S	0	10	0	0	20	0	0	20	0	0	60	0	0	6	0
I-V	0	0	15	0	0	3	0	0	13	0	0	8	0	0	1

* General Average = (Presence Frequency x Arithmetic Average) / 100

the units, including the Triassic, extending in the approximately NNE-SSW direction, particularly around Göksun, appear in red-purple colors. These units consist of Paleozoic-Mesozoic aged metasandstone, quartzite, marble calcschist, gneisses, and granitoids cutting through them. Additionally, a thick limestone layer is tectonically intercalated with metamorphics and sandstone above them. The Upper Miocene-Pliocene aged continental carbonates in the far northwest appear in yellow-green colors. The oldest units, represented by green color, are schists found in the region, while the Quaternary units in and around Göksun, in the far southeast, are depicted in dark blue and its shades. Notably, the marble outcrop just north of the schists is observed in red-yellow colors (Figure 4).

In the ASTER 643 (RGB) combination for Afşin, the marbles in the northwest are clearly seen in red-purple colors, while the green-blue units, especially in the central and southern parts, belong to the ophiolitic mélange. These units mainly consist of neritic limestones, gabbro, and a sheeted dyke complex. In the easternmost region (Ekinözü/Elbistan), metamorphic units predominantly outcrop in blue-red colors, and the green-yellow colors mostly correspond to young continental clastic units. The area south of the Elbistan Fault is characterized by ophiolitic mélange, metamorphics, and granodiorites, with the ophiolitic melangé overlaying the other units tectonically. The active Çardak Fault in an approximately E-W direction, which passes through the south of Ekinözü and is responsible for the second major earthquake that occurred in the region on February 6, 2023, is also included in the image with its distinct linearity.

In the ASTER 12,5,3 (RGB) combination, continental carbonates in Göksun are distinguished by their green color, while marbles and schists are observed in orange-blue-green colors. Alluvium in the Göksun settlement center is represented in khaki color(Figure 5). Afşin and Elbistan regions clearly exhibit greater geological unit

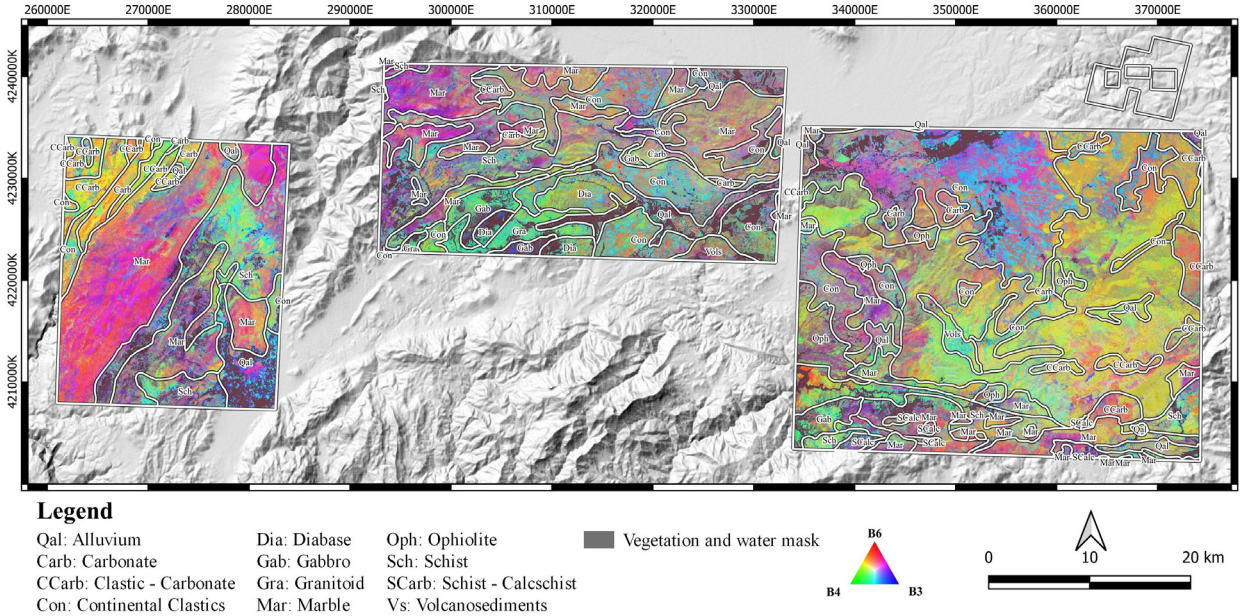

Figure 4. ASTER 6,4,3 (RGB) false color band composite of the studied areas.

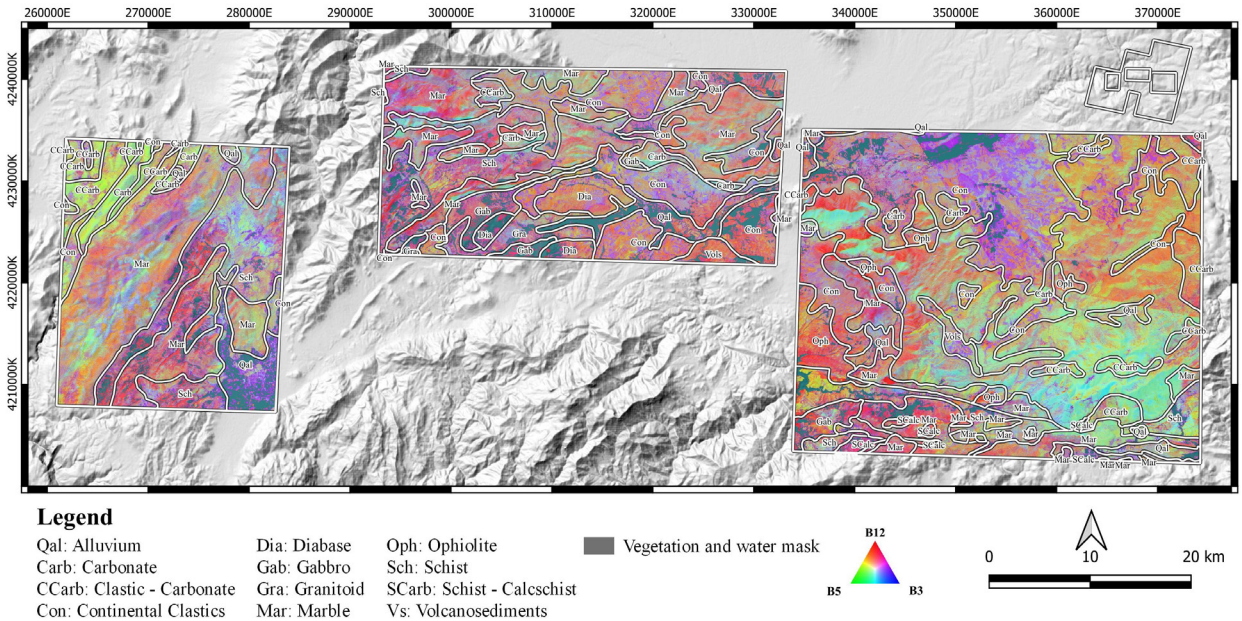

Figure 5. ASTER 12,5,3 (RGB) false color band composite of the studied areas.

diversity in this combination. Likewise, in Elbistan region, it is seen that metamorphics are mostly observed in orange-green colors and carbonates are mostly observed in green color. Metamorphic, magmatic, and sedimentary rocks outcrop in large areas in the region.

ASTER 13, 12, 10 (RGB) image corresponds to a combination consisting entirely of ASTER TIR bands, including the silica and quartz index. Quartz, one of the most common minerals in the Earth's crust, displays absorption in the ASTER's 10th and 12th bands. As a result of this process, in which noise orientations observed in the nature of thermal images are traditionally observed, it is seen that the rocks in Göksun region are mostly metamorphic units and are observed in blue-violet

colors, whereas around Afşin, it is seen that the red-dark pink colors represent the young continental clastics in the region, and the green color mostly represents marbles. The areas represented by green in the south of Elbistan are Triassic aged carbonates and continental clastics, and although the number of lithologies is high due to the ophiolitic complex, full differentiation of units in this region could not be achieved(Figure 6).

5.2. Spectral enhancements

In this method, the aim is to identify the rock units where minerals such as alunite, kaolinite, profillite, epidote, chlorite, amphibole, carbonate, and muscovite—representing the clay and sulfate group—are prominently observed, particularly within the metamorphic rock component and the minerals associated with the geological processes.

5.2.1. Relative absorption band-depth method (RBD)

The method was first described by Brickey et al. (1987) and Crowley et al. (1989) and is similar to the band ratioing method. Its logic involves the use of ratios at the SWIR wavelength that define the depth of the absorption feature at the specific wavelength. Such an image is created by dividing the sum of one or more bands at the centre of the absorption feature, where reflection is minimal (Figure 7).

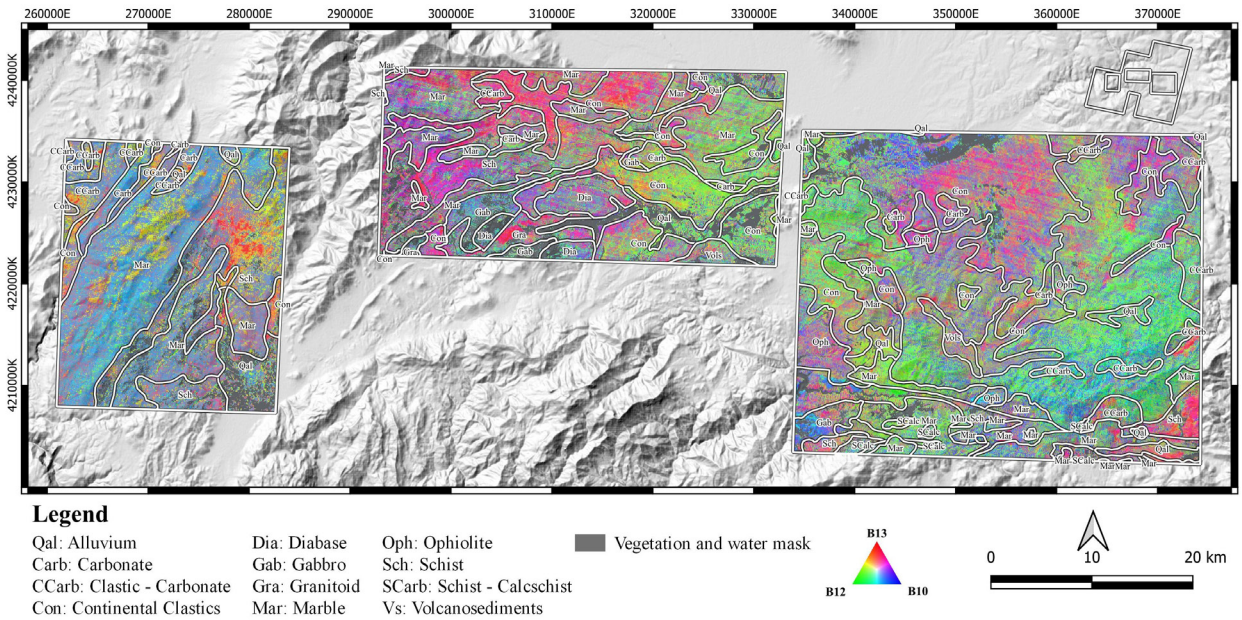

Figure 6. ASTER 13,12,10 (RGB) thermal false color band composite of the studied areas.

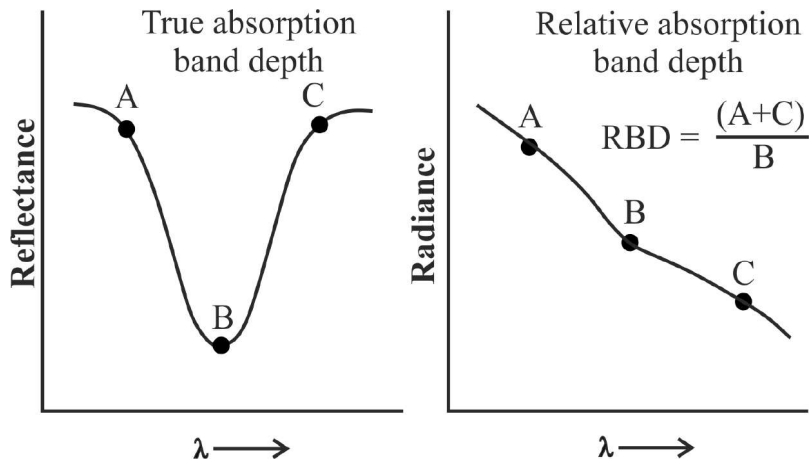

Figure 7. The concept of relative band depth.

Relative band depth, a band ratioing approach, similarly relies on approximating the relative dip in the spectral curve caused by absorption. As illustrated in the figure below, the relative absorption depth at B can be accepted as RBD=h_1/h_2. The spectral ratio calculation is done with a simple three-point formula. The numerator is the sum of the two bands on both ascending shoulders of the spectral curve, while the denominator is formed at the nearest point where the absorption value is at its minimum (Crowley et al., 1989).

Minerals in the AlOH group, such as sericite, muscovite, illite, and Al-smectite, can be distinguished using the ASTER (B_5+B_7)/B_6 band combination (Kalinowski and Oliver, 2004; Hewson et al., 2005; Rowan et al., 2005). In this analysis, with a specific emphasis on sericite and white micas, the 5th and 6th bands encompass the absorption range of profillite and kaolinite. While the 5th and 7th bands of ASTER are located on the absorption edge, the 6th band is above the 2200 nm AlOH absorption value of these minerals. Following this process, AlOH-containing minerals like phengite, muscovite, and smectite can be distinguished from AlOH-containing minerals such as amphibole, chlorite, epidote, and calcite. The 5/7 ratio corresponding to phengite, also known as aluminum-poor muscovite, exhibits a higher reflection compared to the rich kaolinite and muscovite.

These minerals, commonly observed in the study area, particularly in the schists in the Göksun region and the units belonging to the ophiolitic melangé in the south of Afşin, are abundant in the metamorphic units around Ekinözü (Figure 8).

On the other hand, the conditions revealed through the relative band depth method in the regions where kaolinite-alunite and pyrophyllite-rich rocks are common can be observed in Figure 9. According to this figure, notably in the rocks outcropping in the southwest of Afşin and Elbistan, these minerals display very high concentrations. Additionally, concentrations of these sulfate and clay minerals are also observed in other southeast parts.

Similarly, in the implementation of the relative band depth (B7+B9/B8), with the intention of emphasizing carbonate-chlorite-epidote minerals, concentrations were observed in the metamorphic units in the Göksun region. However, this time, it was observed that concentrations were particularly notable in the marbles in the Afşin region and the metamorphic units again in the vicinity of Ekinözü (Figure 10).

In a similar vein, examining another instance of the relative band depth application (B6+B9/B8), targeting concentrated amphibole minerals, reveals extensive outcrops, particularly in the southern region of Elbistan (Hewson et al., 2018). This analysis allows for an approximate estimation of MgOH and carbonate group minerals, relying on the 2.33–2.35 μm absorption characteristic, as illustrated in Figure 11. This relative band depth application is specifically designed for the Afşin region, where rocks belonging to the ophiolitic melangé are concentrated. However, the constrained spectral resolution of the bands in the ASTER SWIR region contributes to certain limitations. Notably, it is evident

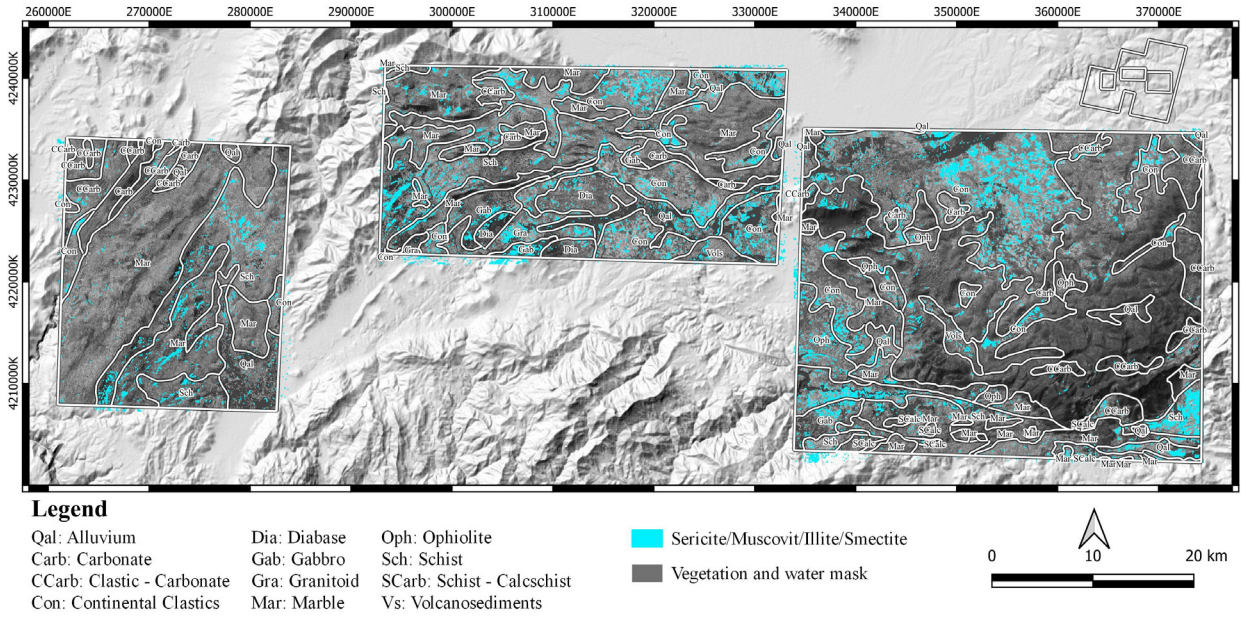

Figure 8. Rock types in which sericite-muscovite-illite-smectite minerals are concentrated according to the relative band depth of ASTER (5+7)/6.

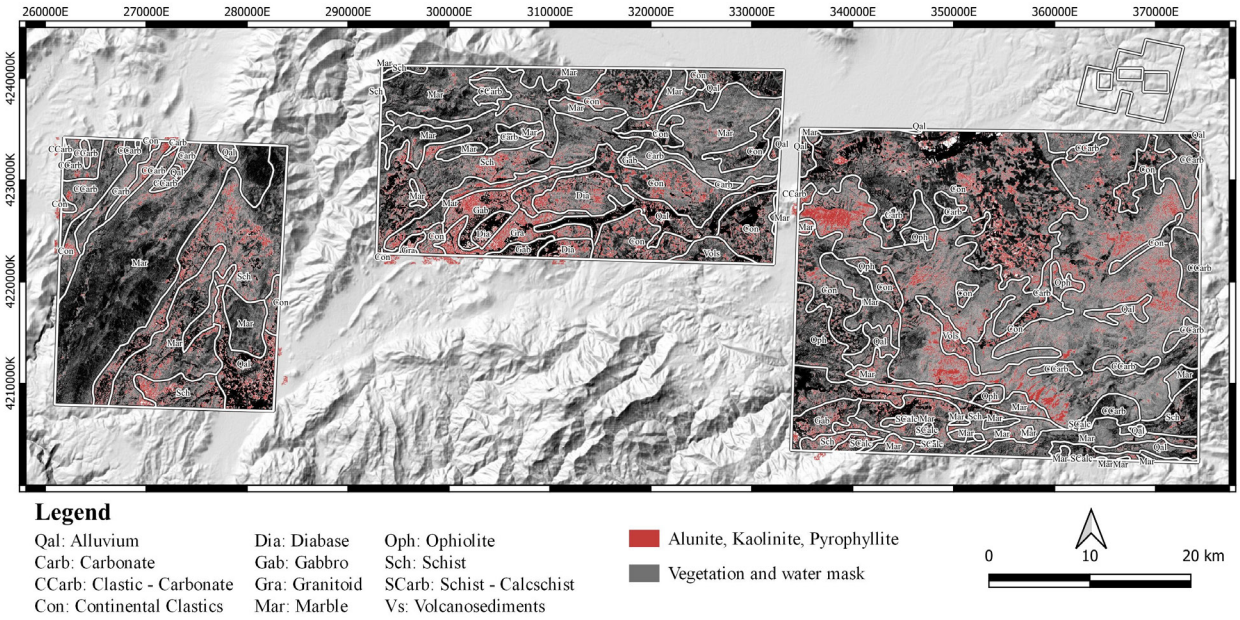

Figure 9. Rock types in which alunite-kaolinite-profillite minerals are concentrated according to the relative band depth of ASTER (4+6)/5.

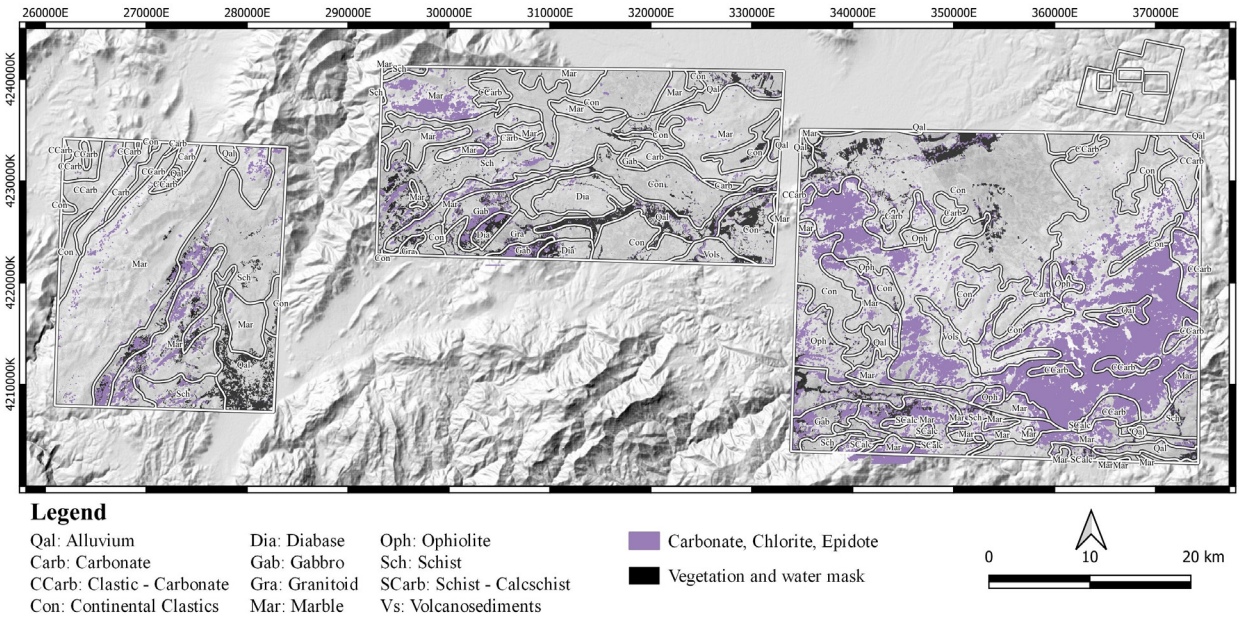

Figure 10. Rock types in which carbonate-chlorite-epidote minerals are concentrated according to the relative band depth of ASTER (B7+B9)/B8.

that epidote-chlorite-amphibole minerals are much more concentrated in these areas compared to other mineral associations. This concentration was observed in marbles to the west in the Afşin region and in marbles, clastics, and carbonates in the Göksun region.Compound products containing MgOH and carbonate content exhibit spectral properties similar to AlOH products. In other words, non-MgOH minerals such as kaolinite and white mica, MgOH minerals such as chlorite and amphibole, and carbonate minerals such as calcite and dolomite present similar compositional information.

In addition to these mineral associations, it was understood that muscovite minerals, which are extensively found in metamorphic units with the B7/B6 band ratio,

are concentrated in marbles and schists in the Göksun region. They are also found in the rocks and marbles of the ophiolitic melangé in the south and southwest, alongside continental clastics in the north derived from metamorphics in the Afşin region. On the other hand, muscovite was widely observed in the schists and calcschists in the south, particularly in terrestrial clastics around Ekinözü (Figure 12).

Analyzing the 13/10 band ratio, commonly referred to as the silica index, constructed using ASTER TIR images and encompassing silica-rich minerals such as quartz, feldspar, and aluminum clays, it can be asserted that rock

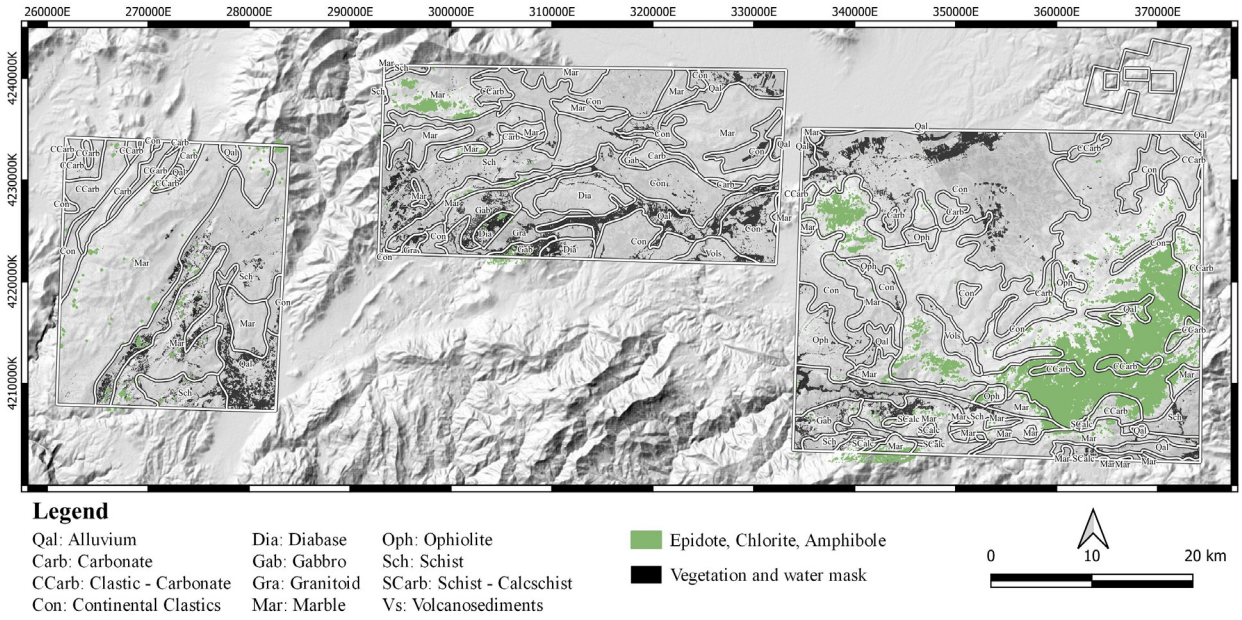

Figure 11. Rock types in which epidote-chlorite-amphibole minerals are concentrated according to the relative band depth of ASTER (B6+B9)/B8.

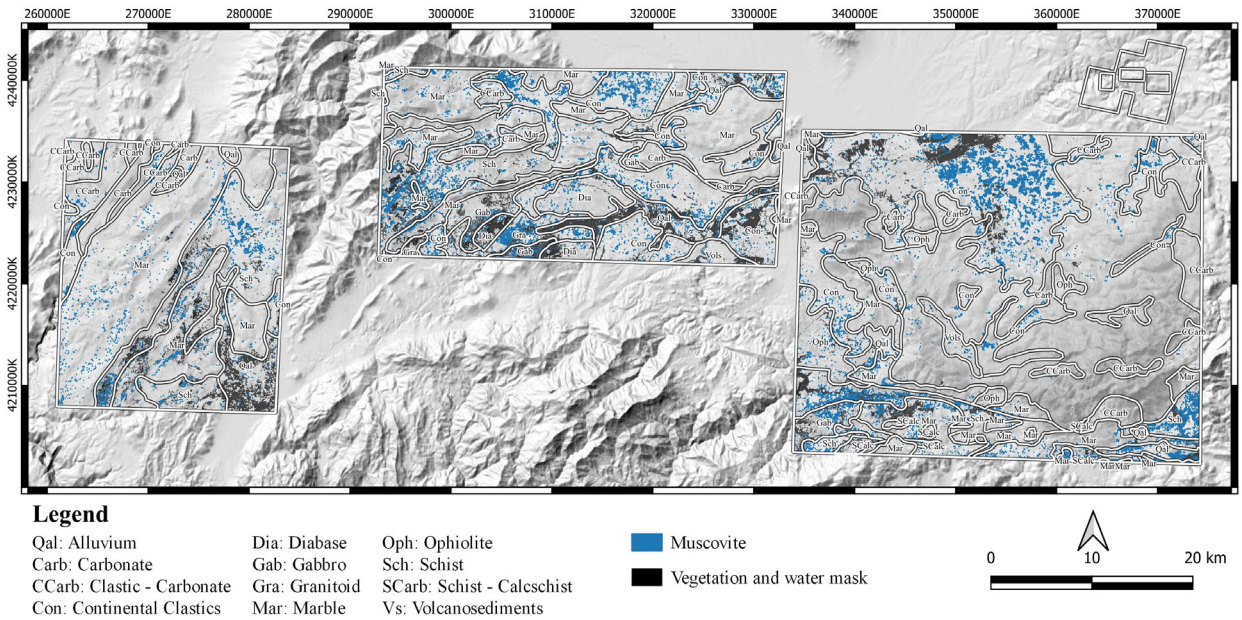

Figure 12. Regions where muscovite minerals are concentrated.

units containing silica are notably concentrated, especially in the schists in the northern part of Göksun and the marbles further west. In the images, black represents water, and vegetation corresponds to the masks. Similar silica-rich content is identified in the units within the ophiolitic melangé, both in the north and south of Afşin. They are concentrated in the schists in the southeast around Elbistan (Figure 13).

5.2.2. Band ratioing combinations

Cudahy and Hewson (2002) suggested some band ratios for biotite-epidote-chlorite-amphibole and garnet-pyroxene and skarn carbonate-epidote indices in rocks with iron oxide, carbonate, white mica, and silica content. In the B4/B7, B4/B3, B2/B1 (RGB) ratio combination (Abrams et al., 1983; Van der Meer et al., 2012), it is seen that marbles and schists are expressed almost as a single unit and cannot show a clear boundary with continental clastics (Figure 14). Likewise, it can be stated that this application does not yield satisfying results in terms of differentiation, not only in the Göksun region but also in the Afşin region. A robust lithological differentiation can be achieved in the units outcropping in the east and southeast of Elbistan. It would be beneficial to review the geological maps used as a reference for further accuracy.

It can be noted that particularly young continental clastics are presented in a bluish-green color, while the units with a yellowish-orange hue located further south consist of metamorphics and clastics-carbonates.

The B4/B3 ratio serves as an indicator for the ferric oxide content of minerals like hematite, goethite, and jarosite. Similarly, the B2/B1 ratio is selected as a compositional ratio chosen for hematite and goethite, corresponding to red and blue colors in this combination. On the other hand, B4/B7 ratio was specifically chosen for direct geological differentiation.

Three different band ratios applied by Volesky et al. (2003), Sultan et al. (1986), and Abrams and Hook (1995) for ASTER data are clearly evident here. The first of these is the B4/B1, B3/B1, B12/B14 combination, with the thermal band ratio targeting silica content added to the combination here. On the other hand, in the other two combinations, the ratio of the 4th and 7th bands forming SWIR bands is represented by the red color. While these bands are known, it can be stated that the combination of Volesky et al. (2003), where the kaolinite mineral is high, is particularly useful for differentiating geological units in the Göksun and Afşin regions.In making this observation, attention is drawn to the presence of numerous distinct colors. On the other hand, it is noted that the combination employed by Abrams and Hook (1995) for the Elbistan and Ekinözü regions produces similarly effective results. In this combination, the B2/B1 ratio for the blue color was utilized to represent ferric iron, proving to be a valuable ratio, particularly for rocks belonging to the ophiolitic complex in the south of Afşin.

5.2.3. Minimum noise fraction (MNF)

The minimum noise fraction transform facilitates the separation of spectral bands dominated by noise from those containing crucial information contributing to the overall dataset mismatch (Figure 15). This process effectively reduces the dataset's size and retains a small number of noise-free pixels (Esmailzadeh et al., 2023). To

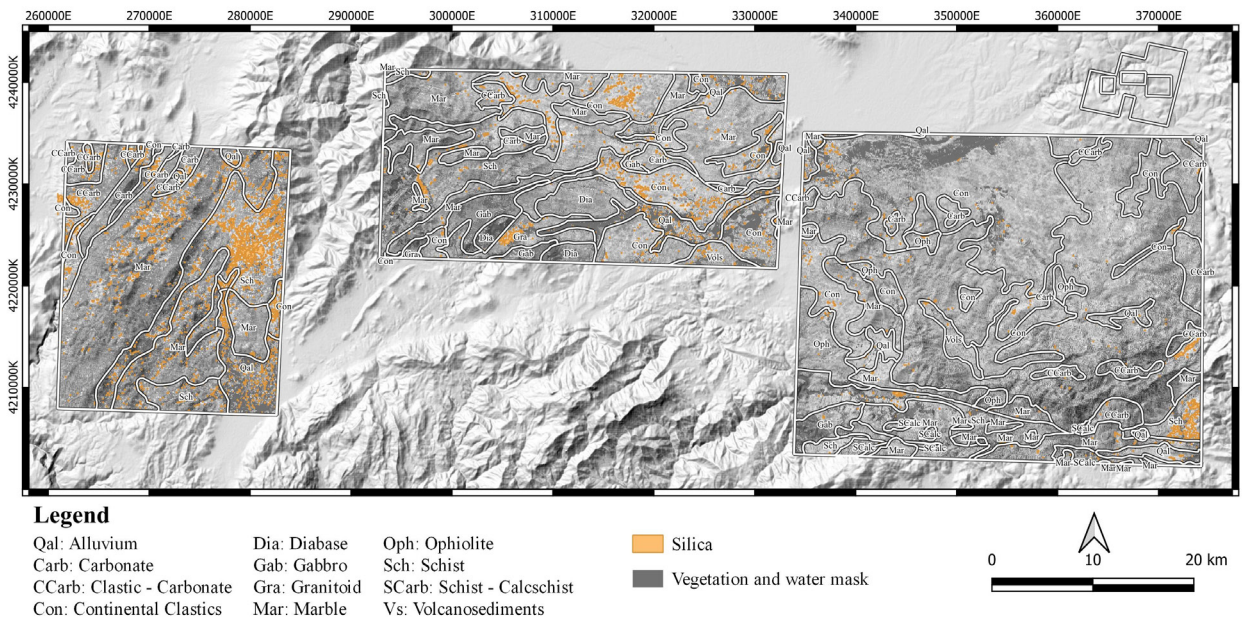

Figure 13. Regions where silica index is concentrated.

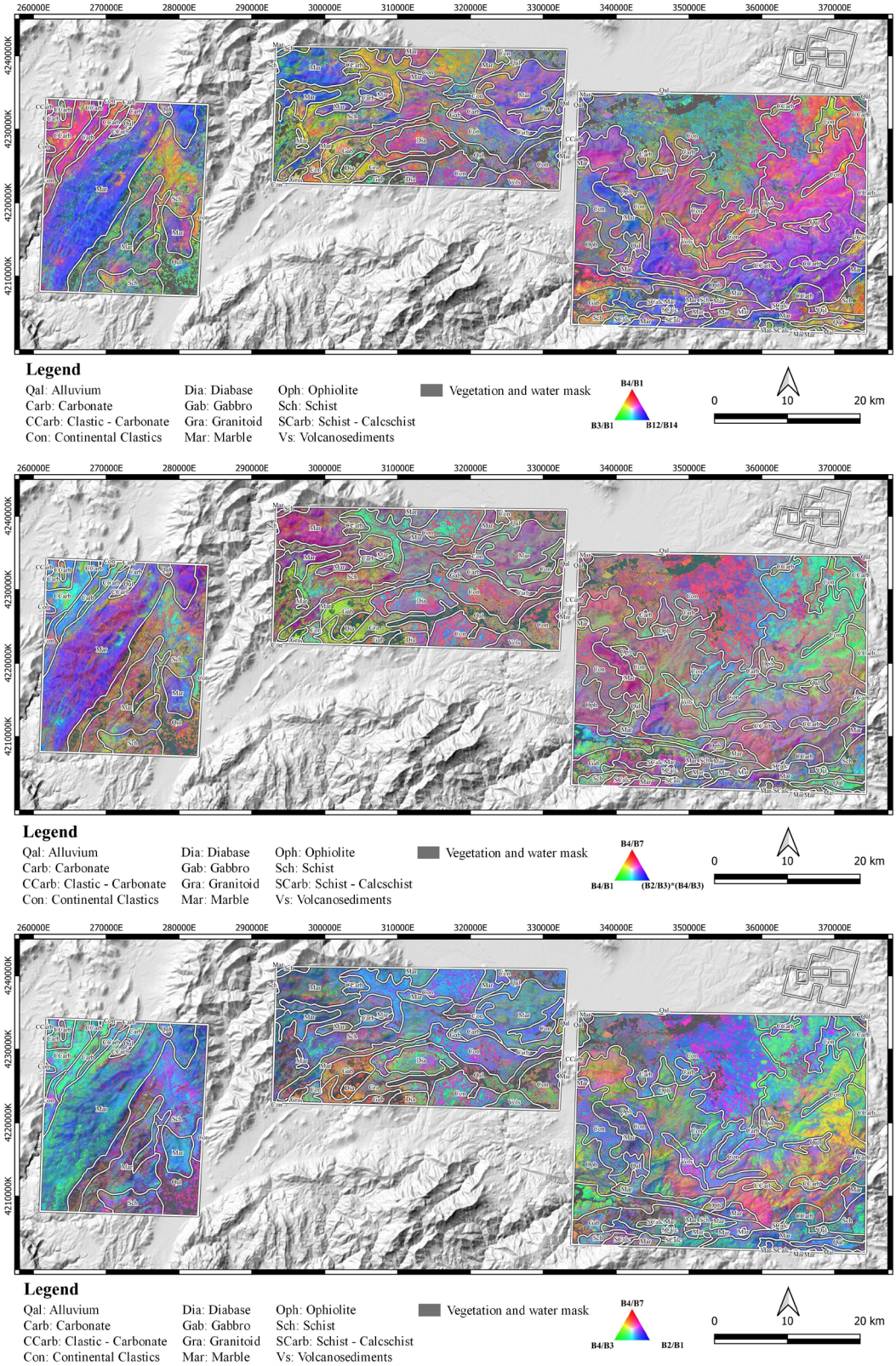

Figure 14. Color composites used by different researchers (Volesky et al., 2003; Sultan et al., 1986; Abrams and Hook 1995) for ASTER images.

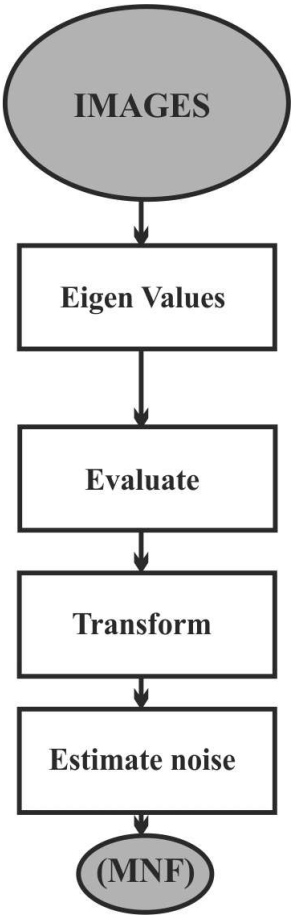

Figure 15. Minimum noise fraction (MNF) process flowchart.

determine the boundary region between signal and noise, it is essential to examine the shape of eigenvalues. The eigenvalues corresponding to the MNF bands, which store information, will have higher magnitudes compared to the eigenvalues for other noise-containing bands. As the eigen numbers increase, the quality decreases; in other words, the amount of noise increases. Therefore, by assessing the eigenvalues, it becomes possible to determine which band gaps are used.

In the context of the minimum noise fraction process, it is noteworthy that among the metamorphics in the Göksun region, marbles are observed in green color, despite the prevailing blue tones, while schists predominantly appear in purple and violet. Conversely, detailed differentiation is not apparent in the continental carbonates in the northwest. In the Afşin region, marbles are noted in green, whereas the ophiolitic rock melangé and continental clastics in the south mostly correspond to purple and violet tones. Notably, the units in the Elbistan region, particularly the southern parts, are prominently and distinctly represented by yellowish-green colors, corresponding to metamorphics and terrestrial clastics among the units in the region. The eastern parts of the district center of Elbistan are clearly distinguished as clastics and carbonates, depicted by purple-violet colors (Figure 16).

6. Discussion and conclusion

Since the ASTER sensor images encompass a total of 14 bands, distributed across three main regions of the electromagnetic spectrum. These include three (3) bands belonging to the visible-near-infrared (VNIR) region, six (6) bands belonging to the short-wave infrared (SWIR) region, and five (5) bands belonging to the thermal infrared (TIR) region. This wide array of bands provides extensive possibilities for combining them into RGB displays to enhance the interpretation and analysis of the captured data. Especially in the SWIR region, the ASTER sensor excels by providing numerous options for geological differentiation. Its capability to generate appropriate color combinations, both independently and in combination with VNIR and TIR bands, significantly enhances its overall performance.

The analyses conducted using the B4/B3 and B2/B1 band ratios revealed areas of iron mineral concentration, including hematite, goethite, and jarosite, with ferric iron content. In contrast, the B4/B7 analysis serves as a ratioing method for geological differentiation. Additionally, the color compound created by assigning the B4/B1, B3/B1, and B12/B14 ratios to red, green, and blue colors aims to differentiate geological units.. In geological remote sensing and image studies, one crucial aspect to consider is the color and tone variations in the image, particularly when interpreting it alongside a geological map. The results of ratios derived from the methods of Abrams and Hook (1995) and Abdelsalam et al. (2000) demonstrated positive outcomes in terms of geological differentiation probabilities for units in the Göksun, Afşin, and Ekinözü regions.

The results obtained from index minerals such as sillimanite, kyanite, staurolite, and garnet in the metamorphic rocks outcropping particularly in the Ekinözü region indicate a medium to high-grade of metamorphism. The band ratioing applications in this study reveal that the metamorphics in the Göksun region can be readily distinguished from other geological units. Analysis of geological maps created in the field suggests that the boundaries between the metamorphics in the Göksun region and the continental clastic units to the east of Elbistan were generally accurately determined through spectral enrichment analyses. In the relative band depth method, recognized for enhancing geological differentiation for minerals and associated rocks with absorption values, particularly in the short-wave infrared (SWIR) region, it is essential to ratio the absorption feature of the selected wavelength (Brickey et al., 1987; Crowley et al., 1989). Through the (B5+B7/B6) process utilizing ASTER bands, the presence of sericite, muscovite, illite, and smectite among the AlOH minerals, along with profillite and kaolinite, was notably observed in the metamorphic units around Ekinözü. This observation extended to units belonging to the ophiolitic complex, especially in the southern region of Afşin. Similarly, in another relative band depth application (B6+B9/B8) aimed at revealing the epidote-chlorite-amphibole content in rocks from the ophiolite complex, it was revealed that this mineral content was extensively observed in the metamorphic rocks of the Göksun and Afşin regions, particularly in the southern part of Elbistan. Extensive observations of carbonate-chlorite-epidote minerals were made in metamorphic units, particularly in the Afşin and Ekinözü regions. Moreover, it was noted that these muscovites were concentrated in the ophiolitic and metamorphic rocks in the Afşin and Göksun regions through the B7/B6 band ratio. In another band ratioing analysis (13/10) performed using thermal bands of ASTER in addition to optical channels, it was understood that quartz, feldspar, and aluminous clays were concentrated in the northern parts of Göksun and Afşin. The minerals revealed through the entire relative band depth method are depicted in different colors in Figure 17, representing their integrated and concentrated localities.

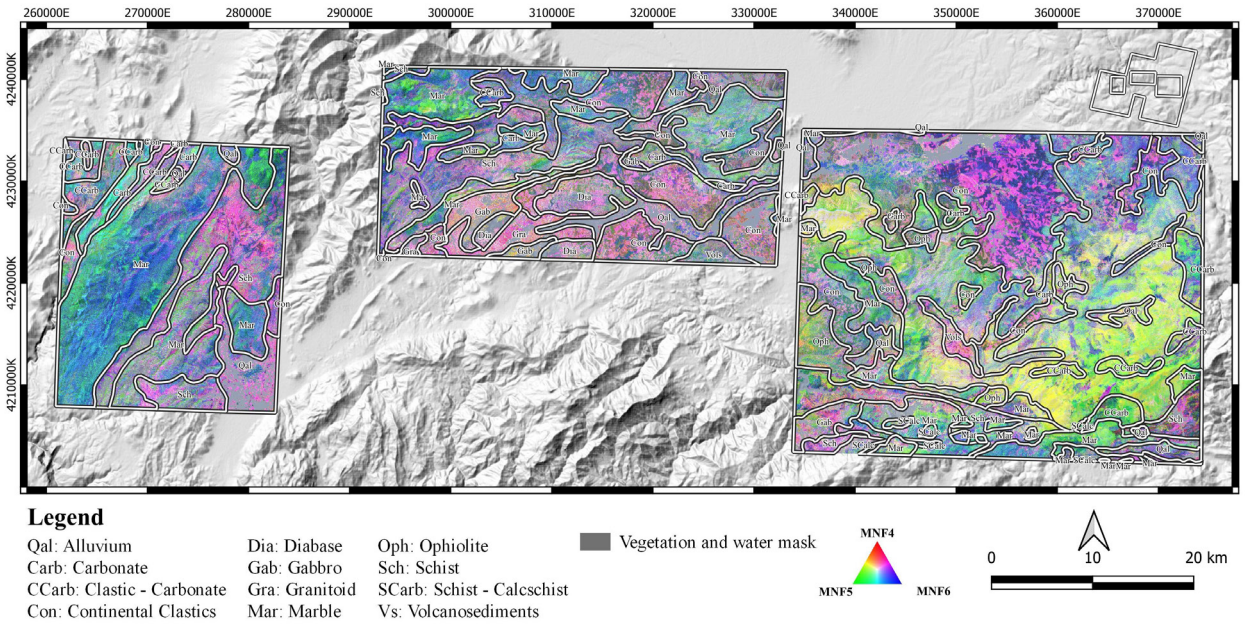

Figure 16. Minimum noise fraction analysis.

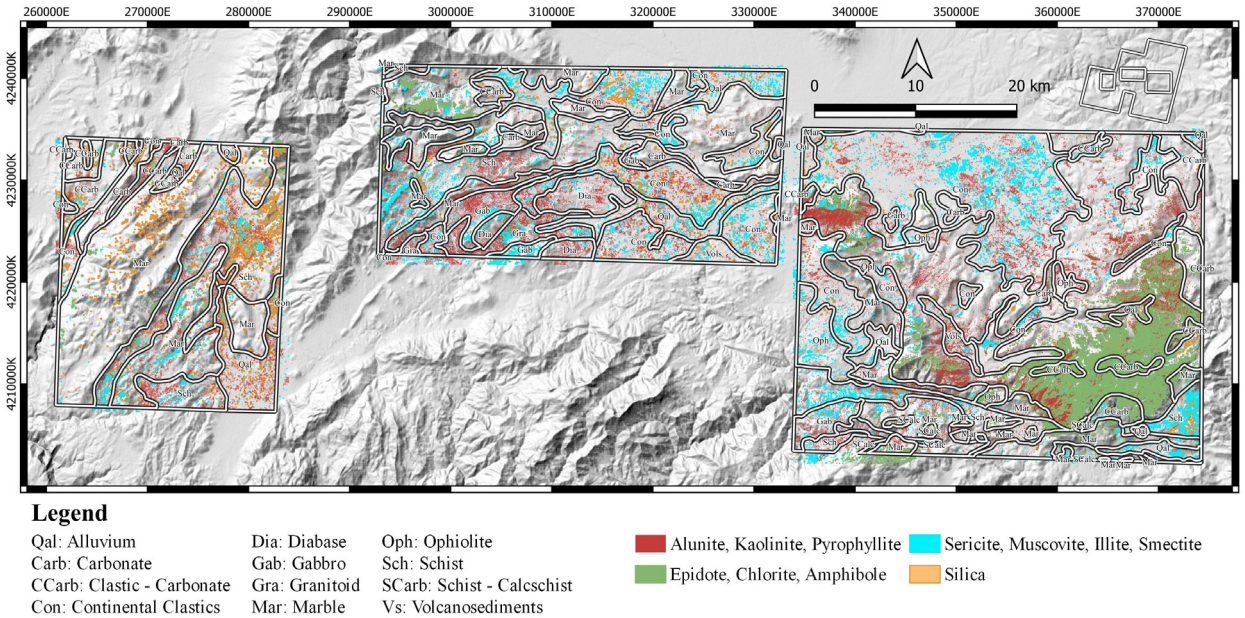

Figure 17. Integrated map showing the distribution of minerals detected by Remote Sensing in the Göksun, Afşin, and Elbistan regions.

To approximate mineral abundances, the study area was divided into three separate areas from west to east: Göksun, Afşin, and Ekinözü. To identify common minerals in these regions, a supervised classification process was employed to emphasize the detected minerals and mineral groups in the images subjected to the relative band depth process. Mineral classifications were derived from the images using pixels (roi) in the parallelogram algorithm previously applied for each mineral and mineral group. The number and percentage of points were calculated for both unclassified and classified points under two groups to determine the mineral abundance in each study area (Table 3).

According to the results, alunite, kaolinite, and pyrophyllite minerals were determined to be 7.938% and 11.149%, respectively, in the Göksun and Afşin sections. In the Ekinözü section, epidote, chlorite, and amphibole minerals were identified as the most abundant, comprising 18.460% of the mineral composition. Evaluating these findings in conjunction with the mineralogical

Table 3. Supervised classification distribution and statistics of minerals detected by remote sensing methods.

Class	**ASTER (Göksun)**			**ASTER (Afşin)**		**ASTER (Ekinözü)**	
	Result	**Npts**	**Pct %**	**Npts**	**Pct %**	**Npts**	**Pct %**
Argillic (Slate for metamorphics rocks) **(Alunite/kaolinite/pyrophyllite)**	Unclassified	2.543.227	92.062	3.120.152	88.851	5.290.857	89.395
	Classified	219.278	**7.938**	391.520	**11.149**	627.683	10.605
Phyllic (phyllite/schist for metamorphics rocks) **(Sericite/muscovite/illite/smectite)**	Unclassified	2.750.395	99.562	3.470.277	98.821	5.856.882	98.958
	Classified	12.110	0.438	41.395	1.179	61.658	1.042
Carbonate/chlorite/epidote	Unclassified	2.732.527	98.915	3.441.696	98.007	5.152.434	87.056
	Classified	29.978	1.085	69.976	1.993	766.106	12.944
Epidote/chlorite/amphibole	Unclassified	2.720.470	98.478	3.420.579	97.406	4.825.999	81.540
	Classified	42.035	1.522	91.093	2.594	1.092.541	**18.460**
Muscovite	Unclassified	2.742.824	99.288	3.463.235	98.621	5.832.306	98.543
	Classified	19.681	0.712	48.437	1.379	86.234	1.457
Silica	Unclassified	2.623.395	94.964	3.453.187	98.335	5.882.870	99.397

composition, metamorphism grade, and data on the rocks' mineralogical composition confirms the presence of very low aWnd low-grade metamorphic rocks containing kaolinite in the Göksun and Afşin regions. In the Ekinözü region, there are low and medium-grade metamorphic rocks containing chlorite and amphibole.

In the image processing analyses conducted using the minimum noise fraction method, it was observed that the metamorphics in the Göksun region could be differentiated from each other based on color differences. However, this differentiation was relatively less pronounced in the sedimentary units, and overall, the method did not achieve a high level of geological differentiation in the ophiolitic, metamorphic, and sedimentary rocks in the region.The data obtained demonstrated that ASTER images can reveal mineralogical and related lithological spatial distributions in regions where mapping is challenging due to geographical conditions. However, it is important to note that ASTER, not being a fully hyperspectral sensor, has limitations in its mineral mapping capacity. Additionally, it is crucial to acknowledge that each landscape has its unique nature, and therefore, the same sensor may not yield identical results for a specific mineral type. Some portions of the geological maps used as a reference may need revision.

Acknowledgment
This study was supported by Sivas Cumhuriyet University Scientific Research Coordinatorship (CUBAP) with project number M-510.

References

Abdelsalam MG, Stern RJ, Berhane WG (2000). Map-ping gossans in arid regions with Landsat TM and SIR-Cimages: The Beddaho alteration zone in northern Eritrea;J. African Earth Sci. 30 (4): 903–916. https://doi.org/10.1016/S0899-5362(00)00059-2

Abrams M (2000). The Advanced Spaceborne Thermal Emission and Reflection Radiometer (ASTER): data products for the high spatial resolution imager on NASA's Terra platform International Journal of Remote Sensing, 21: 847-859. https://doi.org/10.1016/j.jag.2015.01.013

Abrams MJ, Brown D, Lepley L, Sadowski R (1983). Remote Sensing for Porphyry Copper Deposits in Southern Arizona. Economic Geology 78: 591-604. https://doi.org/10.2113/gsecongeo.78.4.591

Abrams M, Hook SJ (1995). Simulated ASTER data for geologic studies, IEEE Transactions on Geoscience and Remote Sensing, 33: 692-699. https://doi.org/10.1109/36.387584

Bailey SW (1980). Summary of recommendations of AIPEA nomenclature committee on clay minerals. American Mineralogist, 65: 1-7.

Bailey EB (1988). X-ray diffraction identification of the polytypes of mica, serpentine, and chlorite. Clays and Clay Minerals, 36: 193-213.

Bierwirth P (2002). Evaluation of ASTER satellite data for geological applications. Consultancy Report to Geoscience Australia.

Bilgiç T (2002). 1/500.000 ölçekli Türkiye Jeoloji Haritaları No:10 Sivas Paftası (Ed.: M. Şenel). Maden Tetkik ve Arama Genel Müdürlüğü Yayınları, Ankara.

Brıckey DW, Crowley JK, Rowan LC (1987). Analysis of airborne imaging spectrometer data for the Ruby Mountains, Montana, by use of absorption band-depth images, Proceedings of the Third Airborne Imaging Spectrometer Workshop, JointNASA-JPL Publication, Greenbelt, Maryland, 87 (30): 143-147.

Brindley GW (1980). Quantitative X-ray mineral analysis of clays: In: Crystal Structures of Clay Minerals and Their X-ray https://doi.org/10.1180/mono-5.7

Clark RN, King TV, Klejwa M, Swayze GA, Vergo N (1990). High spectral resolution reflectance spectroscopy of minerals. Journal of Geophysical Research: Solid Earth, 95 (B8): 12653-12680. https://doi.org/10.1029/JB095iB08p12653

Clark RN, Roush TL (1984). Reflectance spectroscopy: quantitative analysis techniques for remote sensing applications. J Geophys Res, 89 (B7): 6329–6340. https://doi.org/10.1029/JB089iB07p06329

Crosta AP, De Souza C, Azevedo F (2003). Targeting key alteration minerals in epithermal deposits in Patagonia, Argentina, using ASTER imagery and principal component analysis. Int. J. Remote Sens., 24: 4233–4240. https://doi.org/10.1080/0143116031000152291

Crowley JK, Brıckey DN, Rowan LC (1989). Airborne imaging spectrometerdata of the Ruby Mountains, Montana: mineral discrimination using relative absorption band-depth images. Remote Sensing of Environment, 29: 121-134. https://doi.org/10.1016/0034-4257(89)90021-7

Cudahy T, Hewson R (2002). ASTER geological case histories: porphyry-skarnepithermal, iron oxide Cu-Au and Broken hill Pb-Zn-Ag. In Annual general meeting of the geological remote sensing group 'ASTER unveiled', Burlington House, Piccadilly, London, UK.

Drury SA (2001). Image interpretation in geology, 3rd edition, Nelson Thornes, Cheltenham, 304.

Gad S, Kusky T (2007). ASTER spectral ratioing for lithological mapping in the Arabian_Nubian shield, the Neoproterozoic Wadi Kid area, Sinai, Egypt, Gondwana Research, 11: 326-335. https://doi.org/10.1016/j.gr.2006.02.010

Gomez C, Delacourt C, Allemand P, Ledru P, Wackerle R (2005). Using ASTER remote sensing data set for geological mapping, in Namibia. Physics and Chemistry of the Earth 30: 97–108. https://doi.org/10.1016/j.pce.2004.08.042

Green AA, Berman M, Switzer P, Craig MD (1988). A transformation for ordering multispectral data in terms of image quality with implications for noise removal. IEEE Trans. Geosci. Remote Sens. 26: 65–74. https://doi.org/10.1109/36.3001

Gupta R (2018). Remote sensing geology. 3rd ed. Heidelberg: Springer Berlin. https://doi.org/10.1007/978-3-662-55876-8

Hewson RD, Cudahy T, Mizuhiko S, Ueda K, Mauger AJ (2005). Seamless geological map generation using ASTER in the Broken Hill-Curnamona province of Australia. Remote Sensing of Environment, 99 (1–2): 159–172. https://doi.org/10.1016/j.rse.2005.04.025

Hewson R, Van der Werff H, Mshiu E, Alkema D, van der Meer F (2018) Supplementing Geological Mapping with Aster in East Africa," IGARSS 2018 - 2018 IEEE International Geoscience and Remote Sensing Symposium, Valencia, Spain, 8373-8376, https://doi.org/ 10.1109/IGARSS.2018.8519367

Hozatlıoğlu D, Bozkaya Ö, Yalçın H (2021). Geochemical Properties of Phyllosilicates in Goksun, Afsin and Ekinozu Metamorphites (Kahramanmaras, Turkey). Geological Bulletin of Turkey, 64 (1): 41-74. https://doi.org/10.25288/tjb.672813

Hozatlıoğlu D, Bozkaya Ö, Yalçın H, Yılmaz H (2020). Mineralogical characteristics of metamorphic massif units outcropping in Göksun, Afşin and Ekinözü (Kahramanmaraş) region. Bulletin of The Mineral Research and Exploration 162: 105-146. https://doi.org/10.19111/bulletinofmre.610884

Hunt GR (1977). Spectral signatures of particulate minerals in the visible and near infrared. Geophysics, 42 (3): 501-513. https://doi.org/10.1190/1.1440721

Iwasaki A, Fujisada H, Akao H, Shindou O, Akagi S (2001). Enhancement of spectral separation performance for ASTER/SWIR, in Proc. SPIE, San Diego, 4486: 42-50. https://doi.org/10.1117/12.455140

Kalinowski A, Oliver S (2004). ASTER mineral index processing manual. Tech. rep., Geoscience Australia. October 2004.

Luo G, Chen G, Tian L, Qin K, Qian SE (2016). Minimum Noise Fraction versus Principal Component Analysis as a Preprocessing Step for Hyperspectral Imagery Denoising. Can. J. Remote. Sens. 42: 106–116. https://doi.org/10.1080/07038992.2016.1160772

Mars JC, Rowan LC (2010). Spectral assessment of new ASTER SWIR surface reflectance data products for spectroscopic mapping of rocks and minerals, Remote Sensing of Environment, 114: 2011-2025. https://doi.org/10.1016/j.rse.2010.04.008

Mars JC, Rowan LC (2011). ASTER spectral analysis and lithologic mapping of the Khanneshin carbonatite volcano, Afghanistan, Geosphere, 7: 276-289 https://doi.org/10.1130/GES00630.1

Massironi M, Bertoldi L, Calafa P, Visona D, Bistacchi A et al. (2008). Interpretation and processing of ASTER data for geological mapping and granitoids detection in the Saghro massif (eastern Anti-Atlas, Morocco, Geosphere, 4 (4): 736-759. https://doi.org/10.1130/GES00161.1

Ninomiya Y, Fu B, Cudahy T (2005). Detecting lithology with Advanced Spaceborne Thermal Emission and Reflection radiometer (ASTER) multispectral thermal infrared "radiance-at-sensor" data. Remote Sens. Environ., 99: 127–139. https://doi.org/10.1016/j.rse.2005.06.009

Özgül N (1976). Toroslar'ın bazı temel jeoloji özellikleri. Türkiye Jeoloji Kurumu Bülteni, 19: 65-78.

Perinçek D, Kozlu H (1984). Stratigraphy and structural relation of the units in the Afşin-Elbistan-Doğanşehir region. In: International Symposium on the Geology of the Taurus Belt, Tekeli, O. and Göncüoglu, M.C. (Eds.), September 26-29, 1983, Ankara, 181-198.

Pour AB, Hashim M, Hong JK, Park Y (2019). Lithological and alteration mineral mapping in poorly exposed lithologies using Landsat-8 and ASTER satellite data: North-eastern Graham Land, Antarctic Peninsula, Ore Geology Reviews, 108: 112-133, ISSN 0169-1368, https://doi.org/10.1016/j.oregeorev.2017.07.018

Richards JA (1986). Remote Sensing Digital Image Analysis: An introduction. Springer Berlin, Heidelberg, XVII: 281, https://doi.org/10.1007/978-3-662-02462-1

Rowan LC, Mars JC, Simpson C (2005). Lithologic mapping of the Mordor, NT, Australia ultramafic complex by using Advanced Spaceborne Thermal Emission and Reflection Radiometer (ASTER). Remote Sens. Environ., 99: 105–126. https://doi.org/10.1016/j.rse.2004.11.021

Rowan LC, Mars JC (2003). Lithologic mapping in the Mountain Pass, California area using Advanced Spaceborne Thermal Emission and Reflection Radiometer (ASTER) data Remote Sensing of Environment, 84: 350-366. https://doi.org/10.1016/S0034-4257(02)00127-X

Sekandari M, Masoumi I, Pour AB, Muslim AM, Hossain MS et al. (2022). ASTER and WorldView-3 satellite data for mapping lithology and alteration minerals associated with Pb-Zn mineralization, Geocarto International, 37 (6): 1782-1812, https://doi.org/10.1080 /10106049.2020.1790676

Sultan M, Arvidson RE, Sturchio NC (1986). Mapping of serpentinites in the Eastern Desert of Egypt using Landsat Thematic Mapper data, Geology, 14: 995-999. https://doi.org/10.1130/0091-7613(1986)14<995:MOSITE>2.0.CO;2

Şengör AMC, Yılmaz Y (1981). Tethyan evolution of Turkey, a plate tectonic approach. Tectonophysics 75: 181-241. https://doi.org/10.1016/0040-1951(81)90275-4

Ulu Ü (2002). 1/500.000 ölçekli Türkiye Jeoloji Haritaları No:16 Hatay Paftası (Ed.: M. Şenel). Maden Tetkik ve Arama Genel Müdürlüğü Yayınları, Ankara.

Van der Meer FD, Van der Werff HM, Van Ruitenbeek FJ, Hecker CA, Bakker WH et al. (2012). Multi-and hyperspectral geologic remote sensing: A review. International Journal of Applied Earth Observation and Geoinformation, 14 (1): 112-128. https://doi.org/10.1016/j.jag.2011.08.002

Vincent RK (1997). Fundamentals of Geological and Environmental Remote Sensing. Prentice Hall Series in Geographic Information Science. xiii + 370 pp.

Volesky J, Stern R, Johnson P (2003). Geological control of massive sulfide mineralization in the Neoproterozoic Wadi Bidah shear zone, southwestern Saudi Arabia, inferences from orbital remote sensing and field studies. Precambrian Res., 123: 235–247. https://doi.org/10.1016/S0301-9268(03)00070-6

Yalçın H, Bozkaya Ö (2002). Alteration mineralogy and geochemistry of the Upper Cretaceous volcanics around Hekimhan (Malatya), Central East Turkey: an example for the seawater-rock interaction, Bulletin of Faculty of Engineering of Cumhuriyet University, Serie A-Earth Sciences, 19 (1): 81-98.

Yamaguchi Y, Kahle AB, Tsu H, Kawakami T, Pniel M (1998). Overview of Advanced Spaceborne Thermal Emission and Reflection Radiometer (ASTER), IEEE Transactions on Geoscience and Remote Sensing, 36: 1062-1071. https://doi.org/10.1109/36.700991

Yılmaz A, Bedi Y, Uysal Ş, Aydın N (1997). 1/100.000 ölçekli Türkiye Jeoloji Haritası. Elbistan-İ23 Paftası. Maden Tetkik ve Arama Genel Müdürlüğü, 18 s. Ankara.

Yılmaz A, Bedi Y, Uysal Ş, Yusufoğlu H, Aydın N (1993). Doğu Torodlar'da Uzunyayla ile Beritdağı arasının jeolojik yapısı. Türkiye Petrol Jeologları Derneği Bülteni 5: 69-87.

Yılmaz Y (1993). New evidence and model on the evolution of the southeast Anatolian orogen. Geological Society of American Bulletin 105: 251-271. https://doi.org/10.1130/0016-7606(1993)105<0251:NEAMOT>2.3.CO;2

Yılmaz Y (2019). Southeast Anatolian Orogenic Belt revisited (geology and evolution). Canadian Journal of Earth Sciences, 56 (11): 1163-1180. https://doi.org/10.1139/cjes-2018-0170

Yılmaz Y, Yiğitbaş E, Çemen İ (2023). Tectonics of the Southeast Anatolian Orogenic Belt. Compressional Tectonics: Plate Convergence to Mountain Building, 1: 203-222. https://doi.org/10.1002/essoar.10510308.1

Yılmaz Y, Yiğitbaş E (1990). SE Anadolu'nun farklı ofiyolitik-metamorfik birlikleri ve bunların jeolojik evrimdeki rolü. Türkiye 8. Petrol Kongresi Bildirileri, 16-20 Nisan 1990, Ankara, 128-140.